Korea Polymer Journal, Vol. 8, No. 5, pp 224 – 230 (2000)

Relation between Conformational Properties and Yield Behavior of Isotactic Polypropylene under Extension by an Atomistic Modeling Approach

Sung Hoon Yang, Jae Shick Yang, and Won Ho Jo*

School of Materials Science and Engineering, and Hyperstructured Organic Materials Research Center, Seoul National University, Seoul 151-742, Korea

Received August 2, 2000

Abstract : Molecular mechanics technique has been used for finding energy-minimized conformation to understand the mechanism of yielding of glassy polymers in atomistic level. As a model polymer, amorphous isotactic polypropylene (iPP) was generated by molecular mechanics and molecular dynamics methods. The stress-strain curve was successfully obtained by using molecular mechanics technique. The torsional angle distribution showed no significant change during extension, although the torsional angles of certain bonds in polymer backbone changed more largely than other bonds. No significant change in the van der Waals interaction is observed at yielding point, whereas the torsional angle energy starts to decrease at yield strain.

Introduction

Polymers in application ultimately fail by yielding, that is, the onset of plastic deformation. Thus, yielding limits conditions under which polymer materials can be used in load, but at the same time provides for toughness by ductile rather than truly brittle fracture. Although many studies have been devoted to elucidate the nature of yielding, it has not been thoroughly understood at the microscopic level. This is attributed to shortcomings involved in experimental and theoretical approaches. In the experimental approach, microscopic defects in samples makes it difficult to interpret experimental results precisely, while in the theoretical approach, excessive assumptions introduced for simplicity reduce the predictability of the theory. However, atomistic modeling approaches can provide us with useful information on the nature of yielding by controlling shortcomings mentioned above.

Many theoretical approaches to plastic deformation of polymers assume that molecular segment rotation plays an important role in exhibiting yielding.[13,14] However, Utz *et al.*[15] deformed bisphenol-A polycarbonate under compression and found, by solid state NMR, that distribution of torsional angles in polymer backbone does not significantly change during deformation up to strain -0.68. Therefore, the yielding mechanism has still been controversial.

Recently, atomistic modeling techniques have been used to predict and investigate mechanical properties of polymers.[1-12] Suter and his coworkers have predicted mechanical properties of polymers by molecular mechanics.[1-6] In their work, polymeric glasses were viewed as structures trapped in a local minimum of potential energy. They found that the ensemble-average stress-strain curve of glassy polycarbonate exhibits a linear response parallel to the elastic loading line up to about 6% strain, where yielding occurs. Brown and Clarke[6] have simulated a polyethylene-like polymer under tension at various temperatures by a molecular dynamics method. They could observe elasticity, yield, and plastic flow at low temperatures and vis-

*e-mail : whjpoly@plaza.snu.ac.kr

coelasticity at high temperatures by applying uniaxial tension to the system. Fan[9] have studied yielding of glassy polycarbonate under tension using both molecular dynamics and molecular mechanics. He prepared the undeformed structure of polymer in equilibrium by molecular dynamics and simulated its mechanical properties by molecular mechanics. The undeformed structures were extended by changing the cell dimensions in the stepwise manner while the Poisson's ratio was assumed constant. He suggested that the nature of yielding is the inflection exhibited on the Lennard-Jones potential which represents the van der Waals interaction. However, there have been no attempt to clarify the yielding mechanism related with the motion of molecular segments by an atomistic modeling to our knowledge.

In this study, the relation between conformational properties and yield behavior of glassy polymer in amorphous state was investigated using atomistic modeling approach. Isotactic polypropylene (iPP) was chosen as a model polymer because it is widely used for packaging material and has extensively been investigated by computer simulation. The objective of this study is to enhance the understanding of the nature of the yield behavior of glassy polymer. For this purpose, the following procedure is undertaken. First, the deformation of a glassy iPP under extension condition is simulated. The initial structure of iPP is verified in terms of various structural and thermodynamic parameters in comparison with their values obtained from experiments. Secondly, various conformational properties are evaluated to analyze the change in structure and energetic state of iPP during deformation. Thereby, we attempt to clarify the mechanism and nature of yield behavior of iPP.

Model and Simulation Methods

The *Cerius*[2] molecular modeling software from Molecular Simulations Inc. was adopted to build polymers, to perform the energy minimization, and to execute molecular dynamics simulation. In this study, iPP was simulated at glassy state. The model polymer consists of 100 repeating units, corresponding to 902 atoms. The tacticity of polymer chain was controlled by setting meso-diad ratio to be 1.0, i.e., perfectly isotactic. The Dreiding force field[16] was adopted to calculate potential energies between atoms. The potential energy is given as the sum of the following term:

$$E = E_l + E_\theta + E_\phi + E_{inv} + E_{vdW} + E_{Coul} \quad (1)$$

where E_l, E_θ, and E_ϕ are the bond stretching, valence angle bending, and torsional terms, respectively, E_{inv} is the improper out-of-plane interaction, and E_{vdW} and E_{Coul} are the nonbonded van der Waals and Coulomb interactions. The Ewald summation method[17] was used to calculate the nonbonded interaction energies. In Ewald summation, real space cutoff, reciprocal space cutoff, and convergence constant were initially set 6.0 Å, 0.5 $Å^{-1}$, and 2.5 Å, respectively. These parameters were optimized at every 100 time step during simulation.

Initial structures were energy minimized by molecular mechanics. Because these structures might be still in a local energy minimum state, these were relaxed through *NVT* molecular dynamics at 500 K, followed by several alternations of molecular mechanics and *NVT* molecular dynamics at 300 K. The Berendsen thermostat[18] with a coupling constant of 0.1 ps was used to keep the temperature constant. Finally, optimization of structures at fixed angles of simulation boxes was performed: total degrees of freedom in the system were *a*, *b*, *c* and coordinates of atoms. Table I shows the average cell parameters of simulated structures after geometry optimization.

After equilibration and optimization mentioned above, an iPP cell was uniaxially extended along the *y*-axis. The cell was extended by 0.2% of the initial cell dimension, and then relaxed at fixed angles of simulation box by energy minimization

Table I. Average Cell parameters of the Model Polymer

Cell Parameter	Average Value
a (Å)	20.21
b (Å)	20.60
c (Å)	20.18
α (degree)	90
β (degree)	90
γ (degree)	90

using conjugate gradient algorithm.[19] This procedure was repeated until the strain reached 15%.

Results and Discussion

Validation of Simulation. Radial distribution functions were calculated to verify whether the simulated structures have an amorphous nature or not. This function is defined as a probability of finding a pair of atoms at a distance r apart relative to the probability expected for a completely random distribution at the same density. Figure 1(a) shows the radial distribution function of iPP before deformation. The sharp peaks at about 1.1 and 1.5 Å are originated from atomic connectivity, and the peaks at $2\text{Å} < r < 4$ are due to non-bonded atoms separated by two, three, and four bonds on the same chain. From the fact that the value approaches unity at $r > 4$Å, it is obvious that there exists no long-range order in the cell, and thus this structure shows the typical feature of the amorphous state. Note that the amorphous feature of iPP cell remains unchanged after sufficient extension, as clearly seen in Figure 1(b).

The solubility parameter δ is defined as the square root of the cohesive energy density

$$\delta=\left(\frac{E_{Coh}}{V}\right)^{1/2} (\text{J cm}^{-3})^{1/2} \quad (2)$$

where the cohesive energy E_{Coh} is calculated by the energy difference between the isolated chain and the parent chain in the bulk, and is the volume of simulation box. The value of simulated solubility parameter is in good agreement with experimental values, as seen in Table II, indicating that the force field used for this study properly describes the non-bonded interactions.

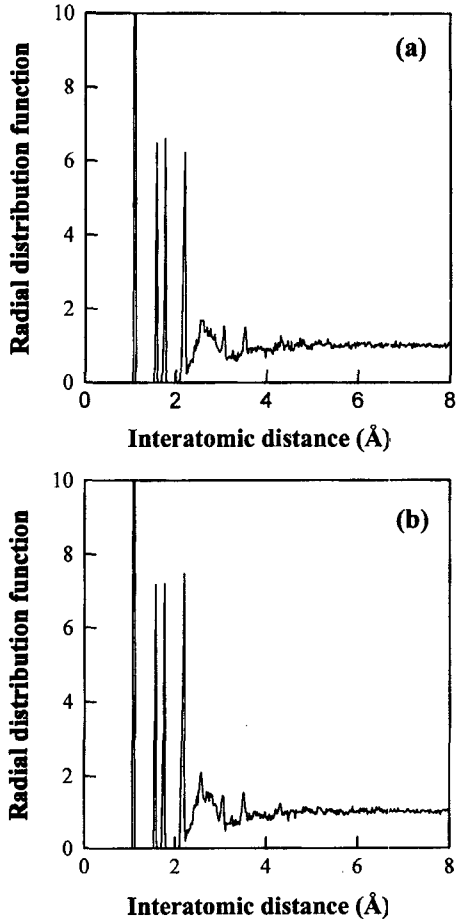

Figure 1. Radial distribution functions for iPP: (a) initial state and (b) after extension.

Plastic Deformation. The stress-strain curve is shown in Figure 2. The internal stress, which is exactly balanced by external applied stress in equilibrium state, can be calculated using the virial theorem.[20] In the virial theorem of statistical mechanics, the stress tensor τ in a macroscopic and bounded system is given in terms of the

Table II. Comparison of Results in This Work with Experiments or Other Simulations

Properties	Other Study		This Work
	Experiment	Simulation	
Density (g cm^{-3})	0.850-0.854[a]	0.892[b]	0.839
Yield stress (GPa)	0.293-0.386[c]	0.14[b]	0.227
Yield strain (%)	11 (at -40°C)[c]	5-7[b]	6.2
Solubility parameter (MPa$^{0.5}$)	16.8-18.8[d]	-	14.7

[a]Ref. (21), from extrapolation of data above melting point.
[b]Ref. (3), atactic polypropylene. [c]Ref. (21). [d]Ref. (22).

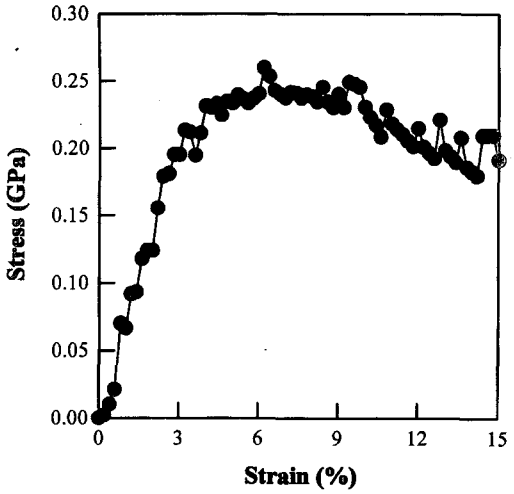

Figure 2. The stress-strain curve of iPP.

atomic momentum p_i, mass m_i, coordinate r_i, and the interatomic force F_{ij} as

$$\tau_{LM}=-\frac{1}{V}\langle\sum_{i}\frac{p_{i,L}P_{i,M}}{m_i}\rangle-\frac{1}{2V}\langle\sum_{i}\sum_{j\neq i}(r_{i,L}-r_{j,L})F_{ij,M}\rangle \quad (3)$$

where bracket denotes an ensemble average, index i runs over all particles 1 through N, and V denotes the volume of undeformed system. In a static, unbounded and periodic model structure, eq (3) can be written as

$$\tau_{LM}=-\frac{1}{2V}\langle\sum_{i}\sum_{j\neq i}(r_{i,L}-r_{j,L})_{min}F^{min}_{ij,M}\rangle \quad (4)$$

where subscript and superscript *min* denotes the distance and the force between minimum-image pairs of atoms, respectively.

In Figure 2, there exists the maximum in stress at ca. 6% strain, which can be considered as the yield point, and thereafter strain softening, i.e., the decrease in stress, takes place. This feature is the same as experiments for amorphous polymers. When the yield stress and yield strain calculated from this simulation are compared with their experimental values as seen in Table II, the value of yield strain obtained from simulation is smaller than the experimental values. This discrepancy may come from the fact that thermal motion is not taken into account during simulation. In other words, mechanical properties of iPP are simulated near 0 K, whereas the experiments are performed at -40 °C.

Simulated mechanical behavior of iPP does not show strain hardening after strain softening, which is known as a general feature for crystalline polymers, although iPP is a semi-crystalline polymer. This is because the simulated model does not contain crystalline parts. However, the model can simulate properly the real system, because it is known that the amorphous region of crystalline polymer responses preferentially under small deformation. Thus it is considered that the initial elastic response and the yield behavior are originated from the amorphous part in crystalline polymers.

The conformation of polymers is determined by the torsional angles of the backbone chain. Consider the rotation of the central bond in a single chain having five repeating units. First, the torsional angle of the central single bond is fixed at 180° and the potential energy is then minimized until the root mean square energy gradient drops below 0.01 kcal $mol^{-1}Å^{-1}$. Starting from this conformation, the central bond is rotated at an interval of 1° while the potential energy is minimized at each step. Several model pentamers were generated for obtaining energy profile, and the energy values were averaged for improving sta-

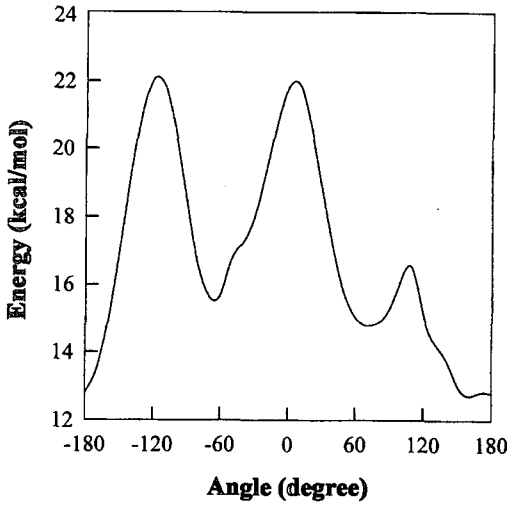

Figure 3. Change of potential energy with torsional angle for the central single bond in a single chain composed of five repeating units.

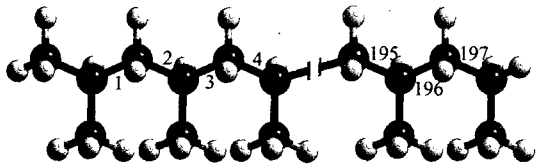

Figure 4. The numbering of the torsional angles in iPP.

tistics of data. The change of the potential energy with rotation of the central bond is shown in Figure 3. Figure 4 illustrates the numbering of torsional angles of iPP backbone. Since the degree of polymerization of iPP is 100, there exist 197 torsional angles of polymer backbone. Figure 5 shows the torsional angle distribution before and after deformation. This distribution is consistent with the results of the energy profile in Figure 3, i.e., larger population at angles of lower energy. It is clear that the torsional angle distribution does not change during deformation, if Figure 5(b) is compared with Figure 5(a).

For the purpose of more detailed analysis, the torsional angle changes of all 197 bonds, as defined in Figure 4, were recorded at every strain step. The $\Delta\phi_{tot}^{(i)}$ in Figure 6 represents the change of torsional angle of i^{th} bond with strain and is calculated by substracting the torsional angle at initial state from that at j^{th} strain step:

$$\Delta\phi_{tot}^{(i)} = \phi^{(i)}(\varepsilon_j) - \phi^{(i)}(\varepsilon_0) \quad (5)$$

where ε_j is the strain at j^{th} step, ε_0 is the strain at the initial state, i.e., zero strain. Figure 6 shows that there are significant changes in some torsional angles, as strain increases. This indicates that all the chain segments do not respond equally: some segments respond more preferentially to the strain than others.

The kinetic behavior of the torsional angles can be monitored by detecting the incremental change of torsional angles at every strain step, as seen in Figure 7. The $\Delta\phi_{step}^{(i)}$ is calculated by substracting the torsional angle at j^{th} strain step from that at $(j+1)^{th}$ strain step:

$$\Delta\phi_{step}^{(i)} = \phi^{(i)}(\varepsilon_{j+1}) - \phi^{(i)}(\varepsilon_j) \quad (6)$$

There are significant changes in some torsional

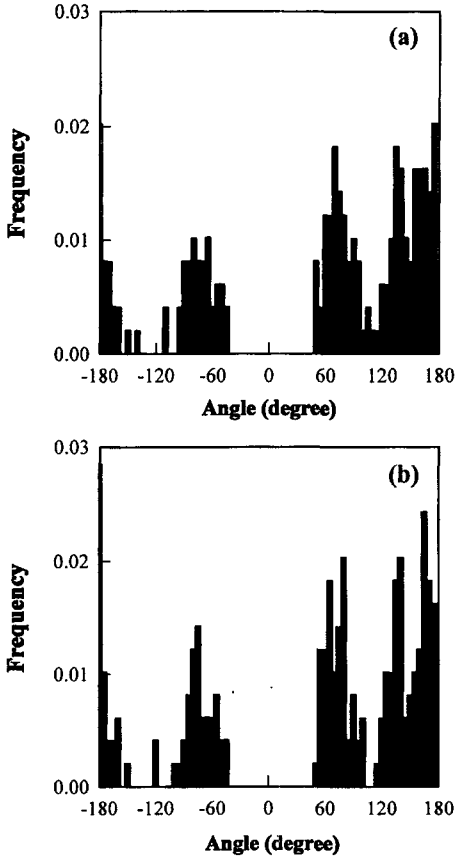

Figure 5. The torsional angle distribution of polymer backbone: (a) initial state and (b) after extension.

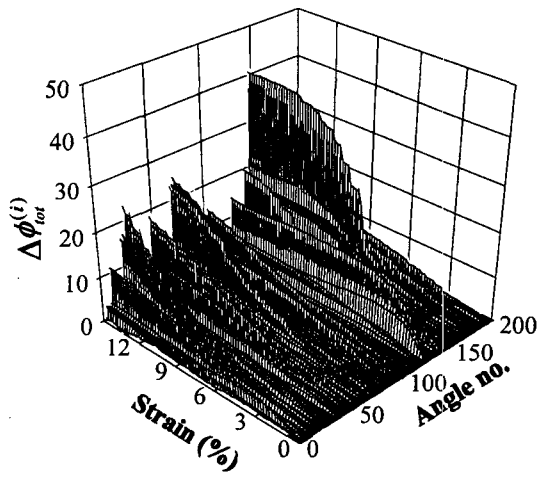

Figure 6. The change of torsional angles of polymer backbone from their initial values with strain.

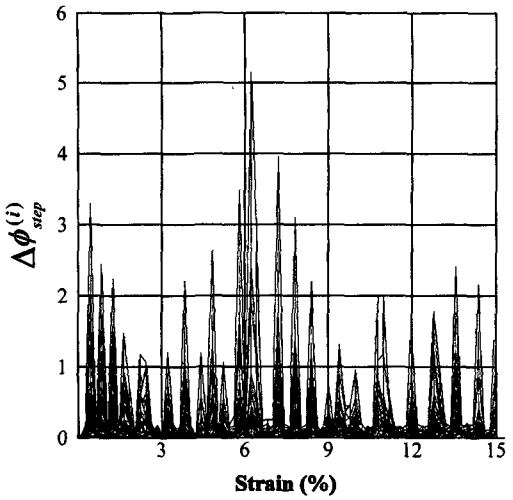

Figure 7. The change of the torsional angles of polymer backbone from those of the previous strain step with strain.

angles at yield strain, i.e., 6%. This suggests that yield is accompanied with torsional angle changes of some bonds in the polymer chain, while the distribution of torsional angles does not change, as shown in Figure 2.

The orientation function, P_2, which is defined as

$$P_2 = \frac{3\langle \cos^2\theta \rangle - 1}{2} \quad (7)$$

where θ is the angle between the segmental vector in backbone chain and an axis. Figure 8 shows that the value of $P_{2\parallel}$ parallel to the extension direction increases, while that of $P_{2\perp}$ perpendicular to the extension direction decreases with increasing strain. Another interesting feature in Figure 8 is that the slope of $P_{2\parallel}$ gradually decreases during deformation. When a glassy polymer is deformed under extension, the chain is oriented to the extension direction until the strain reaches the yielding point. At a yielding point, however, some of torsional angles in polymer backbone change considerably, as shown in Figure 7, which results in the reorientation of segments to an arbitrary direction. As a result, the increase of $P_{2\parallel}$ with strain slows down. The change in energy components is plotted against strain, as shown in Figure 9, in order to analyze the change of energetic state of iPP cell during deformation. The change of total energy with strain is dominantly governed by van der Waals interaction. Nevertheless, no significant change in the van der Waals interaction could be observed at the yielding point. But, the torsional angle energy starts to decrease at the yield strain, as shown in Figure 10.

Conclusions

Mechanical and conformational properties of iPP at glassy state were successfully simulated by an atomistic modeling technique. The equilibrated

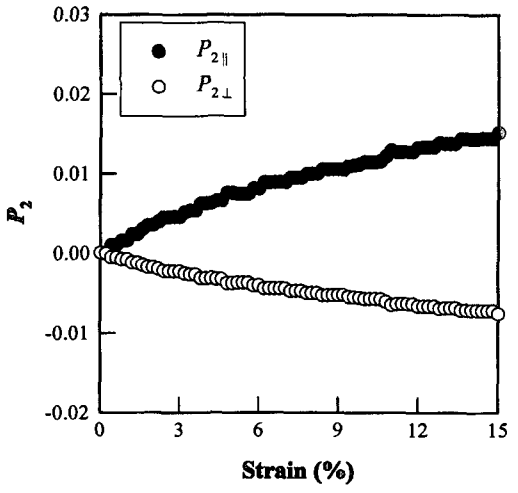

Figure 8. Orientation function as a function of strain.

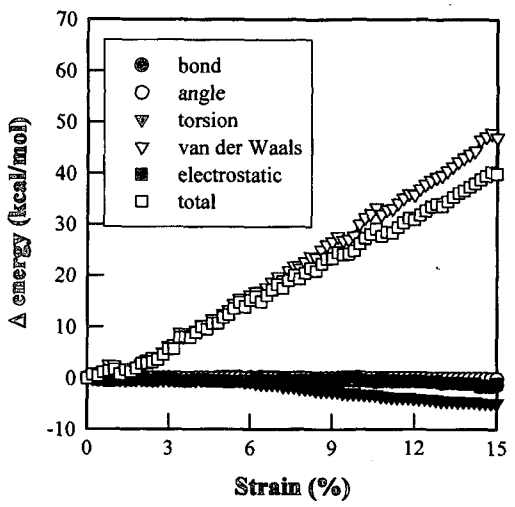

Figure 9. The change of energy components with strain.

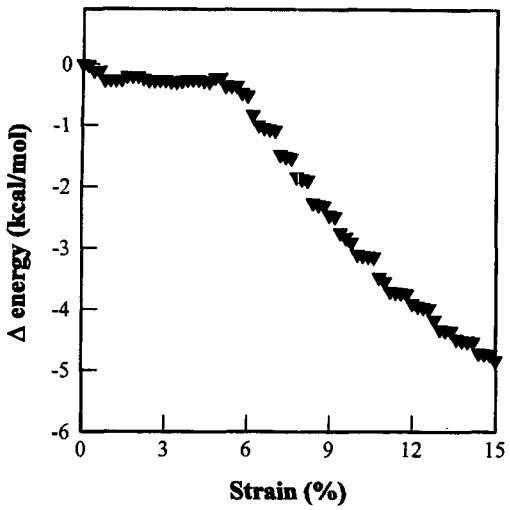

Figure 10. The change of torsional angle energy with strain.

initial structure of iPP was generated using molecular mechanics and molecular dynamics methods. Initial structures represent the amorphous nature, which is confirmed by examining the radial distribution function of iPP. The stress-strain curve obtained from molecular mechanics technique shows the typical features of amorphous glassy polymer, i.e., yielding and strain softening. The torsional angles of some bonds in the polymer backbone change significantly, although the torsional angle distribution of iPP shows no significant change after yielding. The van der Waals interaction does not show a significant change at yielding point, whereas the torsional angle energy starts to decrease at yield strain.

Acknowledgement. The authors thank the Korea Science and Engineering Foundation (KOSEF) for their financial support through the Hyperstructured Organic Materials Research Center (HOMRC).

References

(1) D. N. Theodorou and U. W. Suter, *Macromolecules,* **19**, 139 (1986).
(2) D. N. Theodorou and U. W. Suter, *Macromolecules,* **19**, 379 (1986).
(3) P. H. Mott, A. S. Argon, and U. W. Suter, *Phil. Mag. A,* **67**, 931 (1993).
(4) P. H. Mott, A. S. Argon, and U. W. Suter, *Phil. Mag. A,* **68**, 537 (1993).
(5) A. S. Argon, V. V. Bulatov, P. H. Mott, and U. W. Suter, *J. Rheol.,* **39**, 377 (1995).
(6) M. Hutnik, A. S. Argon, and U. W. Suter, *Macromolecules,* **26**, 1097 (1993).
(7) D. Brown and J. H. R. Clarke, *Macromolecules,* **24**, 2075 (1991).
(8) C. F. Fan and S. L. Hsu, *Macromolecules,* **25**, 266 (1992).
(9) C. F. Fan, *Macromolecules,* **28**, 5215 (1995).
(10) S. S. Jang and W. H. Jo, *Macromol. Theory Simul.,* **8**, 1 (1999).
(11) S. S. Jang and W. H. Jo, *J. Chem. Phys.,* **110**, 7524 (1999).
(12) S. S. Jang and W. H. Jo, *Polymer,* **40**, 919 (1999).
(13) R. E. Robertson, *J. Chem. Phys.,* **44**, 3950 (1966).
(14) A. S. Argon, *Phil. Mag.,* **28**, 839 (1973).
(15) M. Utz, A. S. Atallah, P. Robyr, A. H. Widmann, R. R. Ernst, and U. W. Suter, *Macromolecules,* **32**, 6191 (1999).
(16) A. K. Rappé and W. A. Goddard III, *J. Phys. Chem.,* **95**, 3358 (1991).
(17) N. Karasawa and W. A. Goddard III, *J. Phys. Chem.,* **93**, 7320 (1989).
(18) H. J. C. Berendsen, J. P. M. Postma, W. F. van Gunsteren, A. DiNola, and J. R. Haak, *J. Chem. Phys.,* **81**, 3684 (1984).
(19) W. H. Press, S. A. Teukolshy, W. T. Vetterling, and B. P. Flannery, *Numerical Recipes,* 2nd ed., Cambridge Univ. Press, Cambridge, 1992.
(20) R. J. Swenson, *Am. J. Phy.,* **51**, 940 (1983).
(21) J. Brandrup and E. H. Immergut, Eds., *Polymer Handbook,* 3rd ed., John Wiley and Sons, New York, 1989.
(22) D. W. van Krevelen, *Properties of Polymers,* Elsevier Science Pub., Amsterdam, 1990.